Potential mechanisms underpinning the dissipation of mesoscale eddies over the topographic rise east of the Bahamas

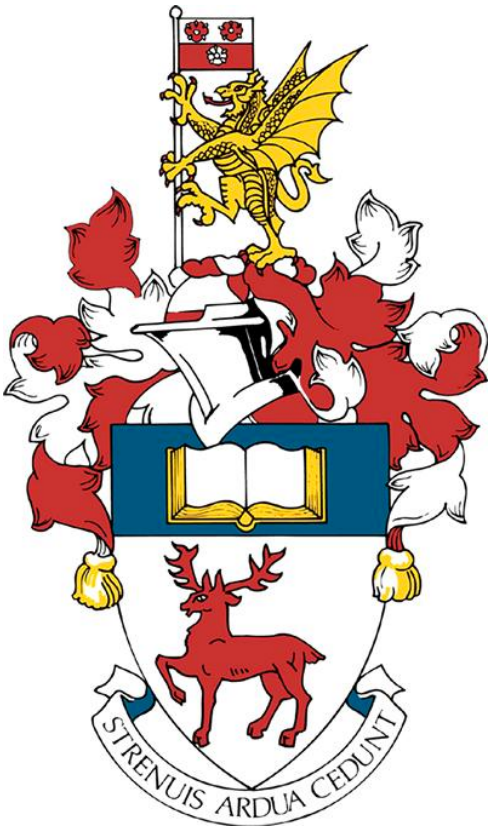

University of Southampton

Faculty of Ocean and Earth Sciences

Jemima Rama

MSci Oceanography/SA

May 2016

Word count: 6700

Abstract

Even if mesoscale eddies represent universal features of the ocean circulation, the processes by which their energy gets dissipated remain poorly understood. This study analyses the spatial distribution of velocity flow and turbulent dissipation rates over the steep topographic rise of Great Abaco, in the Bahamas, to suggest possible mechanisms for eddy dissipation in the area. Data collected from hydrographic cruises as part of the Western Boundary Time Series (WBTS) project is used while the turbulent dissipation rates are estimated using finescale parameterisation. The restriction of high velocity flows to the upper 1000m of the water column suggest that the bulk of the geostrophic flow from the mesoscale eddies cannot penetrate through the permanent pycnocline and hence cannot reach the seabed in the deeper section of the escarpment. The bottom generation mechanisms such as the formation of lee internal waves are only applicable in the shallow section of the topographic rise and not in the deeper section. There is a significant correlation ($r=0.55$) between turbulent dissipation rates and near- bottom current speeds in the shallow area of the continental shelf while this correlation fails in the deeper region. Furthermore, given the distribution of high turbulent dissipation rates within the upper section of the water column, the Kelvin wave hydraulic control might be a potential mechanism for eddy dissipation off the eastern coast of the Bahamas. The meridional velocity of the flows above the pycnocline approaches 0.2m/s, a sufficient speed to excite hydraulic control with respect to local Kelvin waves.

Contents

Acknowledgements

I would like to thank my co- supervisors Eleanor and Alberto for their continuous guidance and encouragement throughout the year. Their enthusiasm about the topic, their feedback and their patience have allowed me to make the most out of this project. I would also like to thank Alex for providing the Matlab codes for finescale parameterisation and for taking the time to introduce and explain the basis of finescale parameterisation as well as Thorpe scales.

1. Introduction

The ocean energy budget involves both mechanical forcing, from the winds and tides (Wunsch & Ferrari 2004), and surface buoyancy forcing (Saenz et al. 2012). While crude estimates of this energy input have been calculated (Huang & Wang 2003) (Munk & Wunsch 1998), large uncertainties still remain on the location and mechanisms through which this energy gets dissipated. Dissipation and diapycnal mixing occur primarily at small scales whereas a significant fraction of the energy input for the ocean happens at large scales. To achieve a balanced energy budget, energy must be constantly transferred to these small scales. Ideally, quantification and a detailed physical understanding of this energy transfer would resolve aspects of the large- scale overturning circulation and would also close model oceanic energy budgets (Ferrari & Wunsch 2009). Furthermore, a dynamical understanding of eddy dissipation would provide the foundations for proper parameterisations of eddies in circulation models. For instance, tuning eddy viscosity coefficients to some preferred outcome most likely diminishes the fidelity of the current models; better parameterisation would account for this issue.

Mechanical and buoyancy forcing drives large- scale slow oceanic motions such as the Antarctic Circumpolar Current, the mid- latitudes gyres and the general overturning circulation. These features are then drained of their energy through geostrophic instabilities to produce mesoscale eddies. Following the combined constraints of conservation of energy and potential vorticity, mesoscale eddies tend to ideally follow an inverse cascade of energy and evolve into larger scales both horizontally and vertically, until they reach an arrest scale (Rhines 1977). The inverse cascade represents the opposite pathway to small scale processes where dissipation by molecular viscosity can occur. Recent altimetric studies (Scott & Wang 2005) have however questioned this inverse cascade, suggesting that a fraction of the eddy

energy follows the direct cascade towards smaller scales and eventually to dissipation and diapycnal mixing. (Zhai et al. 2010) study even highlighted the importance of western boundaries in the oceanic basins as energy sinks for mesoscale eddies; estimating a total of 0.1 to 0.3TW of energy dissipated at the boundaries. However, no scientific study addressed the main physical processes that support eddy dissipation at western boundaries.

As anticipated, the requisite dissipation occurs within the turbulent boundary layer near the surface and bottom. Direct mechanical dissipation of eddies is through damping by the wind stress at the surface (Xu & Scott 2008) while drag acts at the bottom. However, direct frictional interactions with the boundaries and bottom boundary layer are not strong enough to provide the required sink (Dewar & Hogg 2010). In addition, loss of balance is likely to be a small term in the deep ocean (Molemaker et al. 2010). Loss of balance relates to the instabilities of a vertically sheared current; these instabilities can be either gravitational (and convective) following an unstable stratification or centrifugal (and inertial) when there is a change of sign of potential vorticity. The instability processes represent one of the potential routes for the cascade of kinetic energy from the large scales to unbalanced motions at the dissipation scales. Another possible route include the interaction of prexisting inertia- gravity waves with mesoscale motions; such as the capture of wave packet by the eddy field strain (Bühler & McINTYRE 2005).

The most significant pathway for eddy dissipation at western boundaries is most likely the boundary wave generation. When mesoscale eddies impinge on the western boundary, the energy present in the vortices is scattered into high vertical wavenumber modes (Zhai et al. 2010). The boundary generated unbalanced flows can be in the form of internal waves or short Rossby waves for instance. These waves on propagating and subsequently breaking

promote diapycnal mixing and dissipation. Lee internal waves may be generated when geostrophic eddy flows impinge on small- scale rough topography, a phenomenon well documented in the Southern Ocean (Brearley et al. 2013). Additionally, a smooth topography can excite high mode internal waves through hydraulic jumps (Dewar & Hogg 2010). Geostrophic flows along topography tend to trigger the formation of unbalanced Kelvin waves which are thereafter arrested by the balanced flow. The hydraulic control of the Kelvin waves ultimately results in local mixing and internal wave generation.

In view of the boundary wave generation as a mean of eddy dissipation, our study analyses and suggests possible mechanisms responsible for eddy dissipation off Great Abaco in the Bahamas. To achieve this aim, the spatial distribution of turbulent dissipation rates over the topographic rise off Great Abaco is analysed; each dissipation mechanism produces a specific distribution of turbulence and associated diapycnal mixing within the water column. Turbulent dissipation rates are estimated through shear- based finescale parameterization, using data from the hydrographic sections of the Western Boundary Times Series (WBTS) project. (Clément et al. 2015) conducted a similar study in the area and proposed that lee internal wave formation could contribute to eddy decay. High frequency kinetic energy near the seafloor indicated the presence of a bottom generation mechanism when anticyclonic eddies impinged on the western boundary. While (Clément et al. 2015) study was restricted to the shallow section of the topographic rise, this analysis on turbulent dissipation rates extends further offshore and thus encompasses both the shallow and deeper section of the topographic rise. The presence of high bottom turbulence in the deeper section would further reinforce the hypothesis of bottom generation mechanism for eddy dissipation proposed by (Clément et al. 2015) while a different spatial distribution of turbulent dissipation rates would allude to alternative pathways for eddy dissipation. Moreover, a closer examination of the

partitioning of eddy kinetic energy within the water column helps to further understand and explains the dominance of certain dissipative pathways over others.

The paper is structured as follows; section 2 provides an overview of the study region, data collection and processing methods. Section 3 presents the estimates of finescale derived turbulent dissipation rates, alongside the recorded meridional and zonal velocities distributed within the water column. Since the study compares with the bottom generation mechanism found in (Clément et al. 2015), the correlation between bottom turbulent dissipation rates and bottom kinetic energy is also shown in section 3. In light of the partitioning of eddy kinetic energy and associated distribution of turbulent dissipation rates, section 4 discusses the potential candidates responsible for eddy decay processes off the coast of the Bahamas. Section 5 summarises the main findings and proposes alternative methods for a better in-depth analysis of eddy dissipation off the topographic rise of Great Abaco.

2. Data and methods

2.1 Study area

The study was conducted off the steep continental slope east of Abaco Island at 26.5°N, from 77°W and 76.6°W as shown in Figure 1. The study region encompasses the Bahamas escarpment which deepens from 200 m to 4600 m over 30 km. Two upstream ridges protruding from the escarpment, at 26.63°N and 26.73°N respectively and with ridge crests at about 1600m, shield the area from the effects of the southward flowing Deep Western Boundary Current (Johns et al. 2008). The shadow zone provided by the upstream ridges restrict the meridional velocity to less than 0.1m/s at depths below 1600m, with the velocity decreasing closer to topography (Bryden et al. 2005). In the upper 1000m, the thermocline intensified Antilles Current flows northward close to Great Abaco, before joining the Florida

Current. The two currents in conjunction with the Gulf stream forms the northward transport of the North Atlantic subtropical gyre (Lee et al. 1996). In addition, the study region experiences the effects of westward propagating eddies; first baroclinic mode eddies, originating from the open- ocean, impinge on the continental slope (Clément & Frajka-Williams 2014).

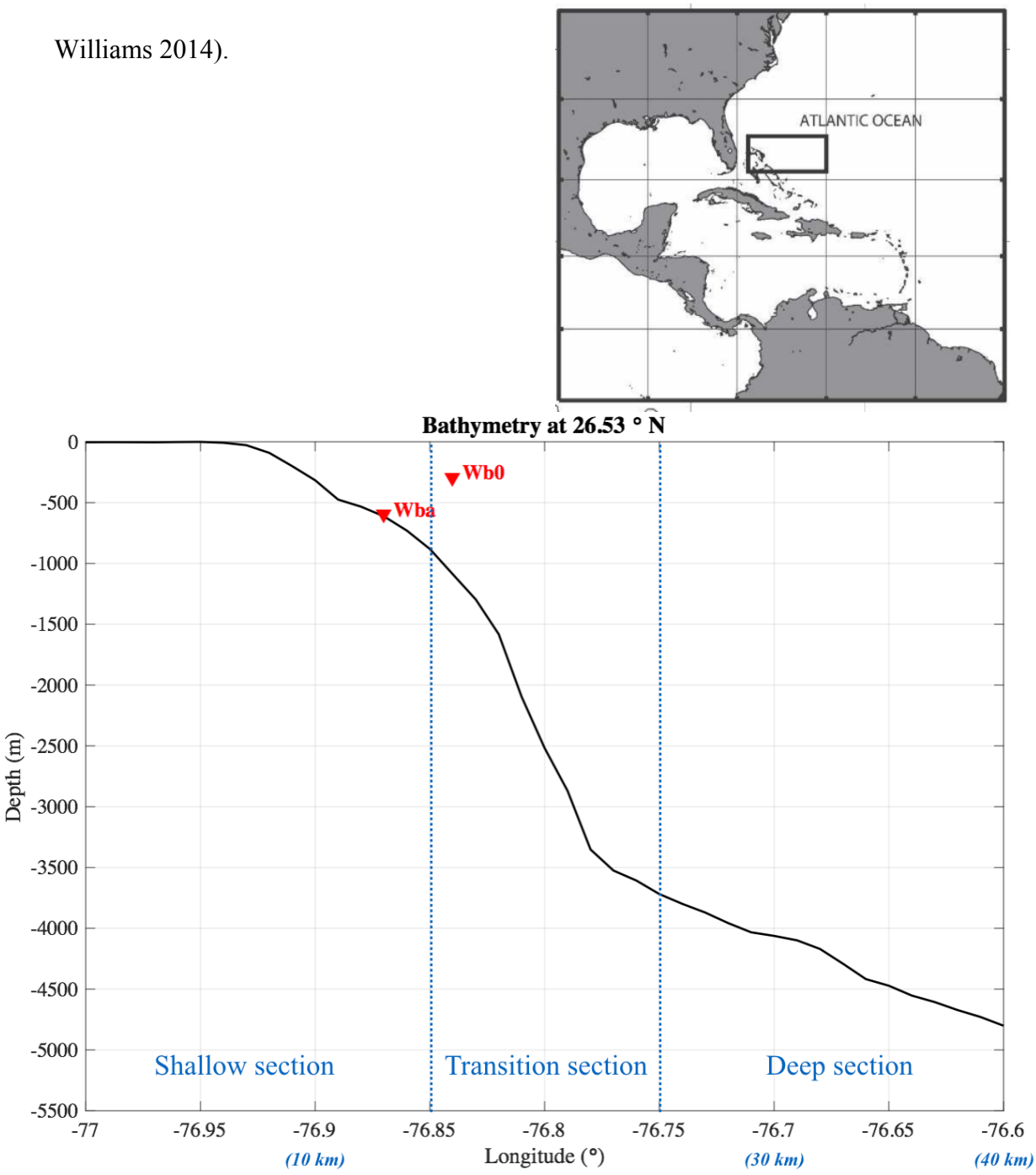

Figure 1:Upper panel: region covered by hydrographic sections of the WBTS. Lower panel: bathymetry of study region. Wba and Wb0 represent the mooring location used in (Clément et al. 2015) *and the dotted vertical lines separate the the study area into three regions depending on their depth.*

2.2 Data acquisition

This study examines the measured finestructure data from hydrographic sections carried under the Western Boundary Time Series project from the National Oceanic and Atmospheric Administration (NOAA). The hydrographic cruises were conducted for a couple of days each year from 2001 to 2015; the specific dates and region sampled by each section is given in the appendix. In order to characterise the internal wavefield and ultimately estimate the turbulent dissipation rates, measurements of temperature, salinity and pressure were obtained from conductivity temperature depth (CTD) while current velocity were acquired from lowered acoustic Doppler current profiler (LADCP). The CTDs employed were Sea-Bird 911plus with a sampling rate of 24 Hz and vertical resolution of O (1 m). The LADCP system consisted of two Teledyne RD ADCPs; a down- looker of 150 kHz and an up- looker of 300 kHz, both mounted on the CTD frame. The LADCP system has a vertical resolution of O (10 m). The description of calibration of instruments and an overview of data processing for the hydrographic sections is available from the respective cruise reports on the NOAA website (ftp://ftp.aoml.noaa.gov/phod/pub/WBTS/Global_Class). Sea surface height anomalies (SSHA) were acquired from AVISO (http://www.aviso.altimetry.fr/duacs/). The bathymetry was obtained from Smith and Sandwell Global Seafloor Topography (http://topex.ucsd.edu/marine_topo/) and was thereafter linearly interpolated onto a finer grid to represent the topography of the study area.

2.3 Finescale parameterization

The use of finescale parameterization to infer turbulent dissipation rates (or associated turbulent diapycnal mixing) relies on the assumption that centimetre- scale dissipation rates can be estimated through quantification of the internal wave shear or strain (Polzin et al.

2014). Through non- linear wave-wave interactions, energy cascades down from the internal wave field in the large vertical scale towards dissipative small scale disturbances. The small instabilities increase the shear variance until it overcomes the stratification, allowing the internal wave to break and cause diapycnal mixing. Given a statistically steady or slowly varying wavefield, the rate at which wave breaking dissipates energy is similar to the rate of energy transfer from large to small scales (Gregg et al. 2003). Therefore, the estimated amount of energy present in the internal wavefield is approximately similar to amount of energy available for diapycnal mixing.

The indirect estimates of turbulent dissipation rates, ε are computed by comparing the observed shear spectral variance to that of the background internal wavefield in the open ocean; the latter is given by the Garrett- Munk (GM) model. ε is calculated following the detailed equations given in (Polzin et al. 2014) with the general formula for the rate of turbulent production from vertical profile measurements being ;

$$\varepsilon = \varepsilon_o \frac{f}{f_o} \frac{N^2 \cosh^{-1}(N/f)}{N_o^2 \cosh^{-1}(N_o/f_o)} \hat{E}^2 \frac{3(R_\omega + 1)}{4R_\omega} \sqrt{\frac{2}{R_\omega - 1}} \qquad (1)$$

where ε_o is the reference GM dissipation rate set to $6.73\times10^{-10} Wkg^{-1}$, N_o is the GM stratification set to $5.24\times10^{-3} s^{-1}$ and f_o is the reference Coriolis factor for 26.5°N. The shear- to strain variance ratio, R_ω which defines the internal wave field's aspect ratio and its frequency content (Kunze et al. 1990) is set conservatively to 7. All the above mentioned constants are set to the same values as in (Clément et al. 2015) so that the findings of the latter in the shallow section of the topographic rise off Great Abaco can be compared to the results of this study.

N^2, the buoyancy frequency, relates to the water stability and is calculated from the density (ρ) derived from the CTD temperature and salinity measurements at each station. ρ_o is the reference density, calculated as the mean of all measured ρ.

$$N^2(z) = -\frac{g}{\rho_o}\frac{\partial \rho(z)}{\partial z} \qquad (2)$$

The factor $\hat{E}$ represents a band- limited estimate of the shear spectral density relative to the high- wave number asymptote of the GM spectrum. A detailed explanation for the computation of $\hat{E}$ can be found in (Polzin et al. 2014).

The shear variances, $\langle V_Z^2 \rangle$ are calculated from the integrated buoyancy frequency- normalised observed shear spectrum and GM shear spectrum respectively, in the vertical wavenumber space. The vertical shear profiles are first divided into 240 m half- overlapping bins. The shear (V_z) is normalised to the mean buoyancy frequency ($\overline{N}$), tapered using Hann window function and then Fourier transformed to produce the shear power spectra. Following the equations given in (Polzin et al. 2002) spectral corrections are applied; range averaging for vertical smoothing of data, first- differencing to remove unknown package motion and interpolation associated with bin mapping to account for instrument tilt.

The spectra, $S[V_z/\overline{N}]$ are then integrated from a minimum vertical wavenumber (min k_z corresponding to wavelength, λ_z = 200 m) to a maximum wavenumber (max k_z corresponding to λ_z = 90 m). (Kunze et al. 2006) demonstrated that the upper bound for shear variance integration should be set to a maximum k_z corresponding to a minimum λ_z =

100 m. At higher wavenumbers (or correspondingly lower wavelengths), the shear spectrum is contaminated by LADCP noise and could thus result in an overestimation of the shear variance. The effect of noise contamination is shown in Figure 2, whereby the shear variance spectrum for λ_z < 100 m exhibits spikes and does not mimic the shape of the reference GM shear variance spectrum. The integration limits (vertical dotted lines in Figure 2) are chosen so as to encompass the shear spectrum section least affected by the noise. The vertical bounds are also limited at lower wavenumbers (higher wavelengths) by the spectral drop off and limitations to evaluating depth variability within each profile if spectra are calculated over a too large depth range.

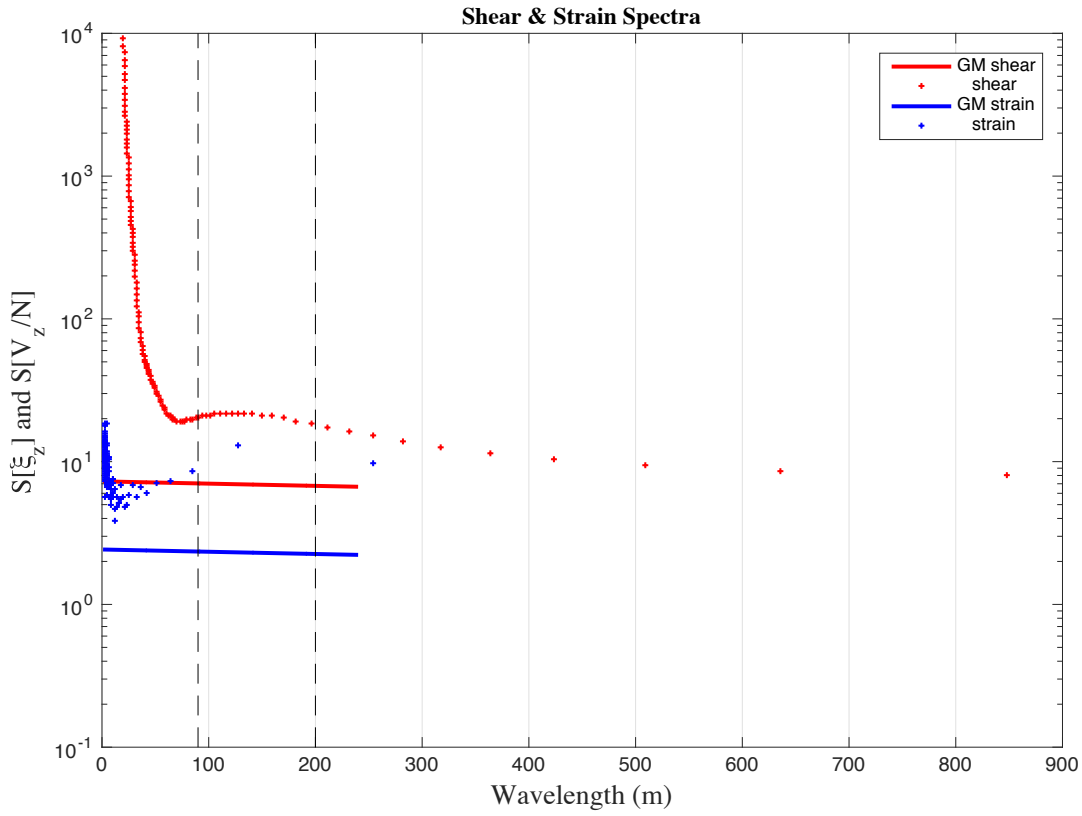

Figure 2: Shear (red) and strain (blue) power spectra averaged over the numerous vertical depth bins. The thick lines are the spectra from the reference GM spectrum while the scatter plot represent the spectra computed from measured data.

In addition, shear based finescale parameterisation is used in this study as opposed to strain based finescale parameterisation. Strain (ξ_z) is computed as the perturbation in the local stratification and hence uses measurements from the CTD. However, CTD strain variances

tend to get contaminated by background stratification at λ_z > 150 m and in the presence of sharp pycnoclines (Kunze et al. 2006). The strong seasonal and permanent pycnoclines off the Bahamas (Clément & Frajka-Williams 2014) contaminates the CTD strain variances as exhibited by the substantial spike at wavelengths, λ_z < 100 m (Figure 2).

2.4 Thorpe scales

On a side note, Thorpe scales as described in (Park et al. 2014) and (Gargett & Garner 2008) were also used to infer the turbulent dissipation rates within the study area. However, given the inconclusive nature of the turbulent dissipation rates from Thorpe scales, the latter were not presented in this paper. Thorpe scale produces better estimates of turbulence when applied to density profiles obtained from a specialised free- falling profiler (Polzin et al. 2014). Since Thorpe scales rely on the detection of overturns within the water column, questionable instabilities related to ship motions, in instances of swells, or to water entrainment by the wire lowered CTD can introduce false overturns into the density profile. Computation of an intermediate density profile as proposed by (Gargett & Garner 2008) for Thorpe scales allows the removal of the false instabilities. The latter however conducted their study in a very energetic environment with vigorous meaning defined by vertical scale overturns of *O*(10- 100m); such large overturns tend to be less affected by noise contamination (Polzin et al. 2014). The study region off the Bahamas is not as turbulent. The calculation of the intermediate density profile might not completely resolve noise contamination produced by the ship motion and wired CTD package. In addition, before calculating Thorpe scales, (Park et al. 2014) used a series of procedures to account for the thermal lag and salinity spiking caused by the differing time responses of temperature and conductivity sensors. For this study the available CTD data was already processed and it is

uncertain if the above mentioned steps were applied correctly to the raw data so as to minimise the effects of instrument noise.

2.5 Vertical modes

In order to acquire a better understanding of the eddy kinetic energy and their variability with depth, the dynamical modes near the study area are analysed. Stratification strongly alters the mode shapes and various forms of mode can exist depending on the assumptions made. In this case, the simplest theoretical assumptions are applied; an ocean with flat bathymetry, no background motion and fixed boundary conditions (rigid lid condition at surface and bottom of the ocean). The modal structures are determined from (Gill 1982) using a finite differencing scheme of the Sturm- Liouville equation;

$$\frac{d^2 F_m(z)}{dz^2} + \frac{N^2(z)}{c_m^2} F_m(z) = 0 \qquad (3)$$

The zeroth- mode $(m = 0)$ represents the barotropic mode, $m = 1$ is the first baroclinic mode, $m = 2$ is the second baroclinic mode and so forth. The eigenvalue c_m is the phase speed of the mode-*m* gravity waves. The eigenvalue relates to the Eigen function, that is normal modes, $F_m(z)$. $N^2(z)$ is the mean buoyancy frequency profile, computed from all the stations. Given the above mentioned assumptions, the boundary conditions are set as $F(z) = 0$, at $z = 0$ and $z = -H$. In order to solve for the Eigen values and corresponding Eigen functions, a coefficient matrix is created; the mean buoyancy frequency of each defined layer is along the diagonal of the symmetric axis.

3. Results

Using shear based finescale parameterisation, turbulent dissipation rates for each hydrographic section is calculated and plotted. SSHA from satellite altimetry data is shown while velocity flows are plotted from LADCP measurements. Figure 3 represents data from only one hydrographic section. A selection of graphs from the 15 hydrographic sections, is presented in the appendix. All the hydrographic sections demonstrate the same spatial distribution of ε, u and v as in Figure 3. High velocities, especially in the meridional ($|v| > 0.2m/s$), are restricted to the upper 1000 m of the water column. Similarly, high turbulent dissipation rates of $O(1\times10^{-10}\ W\ kg^{-1})$ are confined to the upper 1000m while turbulent dissipation rates are only of $O(1\times10^{-11}\ W\ kg^{-1})$ below this depth. It is essential to note that the calculated turbulent dissipation rates have not been validated against direct microstructure measurements and may not provide accurate estimates of turbulence. In fact, shear- based finescale parameterisation become erroneous near topographic features (Hibiya et al. 2012). At continental shelves for instance, the internal wave spectrum gets distorted and deviates from the GM spectral shape. The shelf internal wave field does not satisfy bandwidth assumptions (Kunze et al. 2006), causing finescale parameterisation to either underestimate or overestimate the turbulent dissipation rates. However, the principal motivation of this study is to investigate the spatial distribution of turbulent dissipation rates and not to quantify the later. No frequency based correction, in the form of vertical shear to vertical strain ratio of the local internal wave field, (Polzin et al. 1995) is applied to account for the overestimation (or underestimation) of the finescale derived turbulent dissipation rates. Readers should not focus on the quantification of the turbulent dissipation rates but rather on the variation of turbulent dissipation rates over the topographic rise. In this paper, the order of magnitude of turbulent dissipation rates are only mentioned to better compare regions of high and low turbulent dissipation rates.

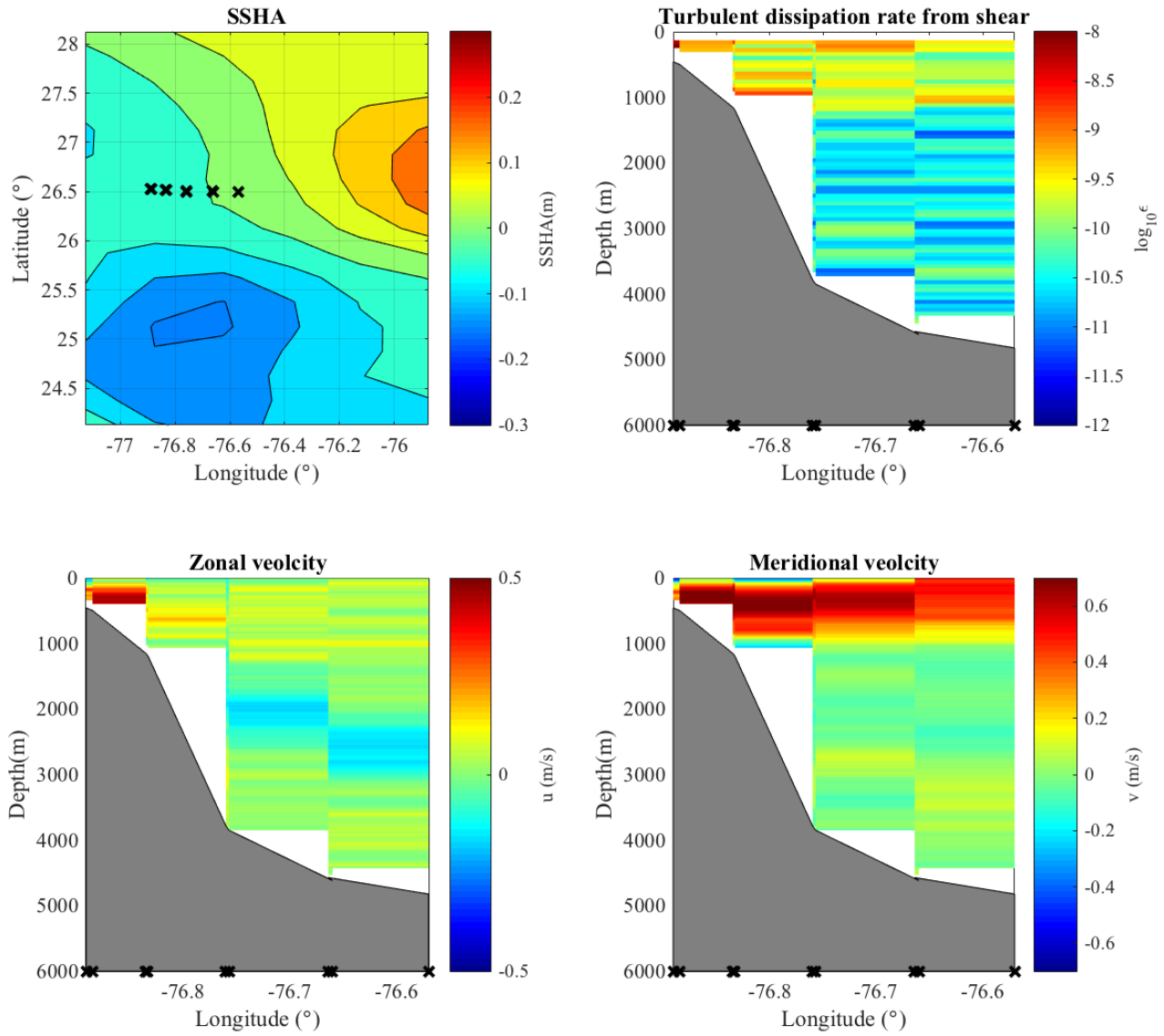

Figure 3: SSHA, turbulent dissipation rates, meridional and zonal velocity from the hydrographic section of May 2005. The black crosses indicate the location of the stations. In this case, an anticyclonic eddy is seen approaching Great Abaco. High meridional velocity is recorded in the upper 1000m and relatively high estimates of turbulent dissipation rates is observed in the upper 1000m of the water column.

Since higher turbulent dissipation rates across all transects appear to be associated with regions of higher current speeds, the correlation between turbulent dissipation rates (ε) and kinetic energy (KE) is analysed. (Clément et al. 2015) suggested a bottom generation mechanism for the dissipation of eddies; to further investigate the findings of their study, ε and KE are vertically averaged over the bottommost 100 m of the water column. The averaged values from the bottommost 100 m of the water column are defined as $\langle KE \rangle$ and

$\langle\varepsilon\rangle$. The correlation analysis between $\langle KE\rangle$ and $\langle\varepsilon\rangle$ is done separately for 3 sub-sections of the study area. Given the steep escarpment, the study area is divided into 3 regions (Figure 1); the 'shallow' region extends from 77°W to 76.85°W (maximum depth of 1000 m), the 'transition' region with the large drop off extends from 76.85°W to 76.75°W (maximum depth of 3500 m) and the 'deep' region extends from 76.75°W to 76.6°W (maximum depth of 4500 m). Figure 4 shows the local relationship between the bottom turbulent dissipation rates, $\langle\varepsilon\rangle$ and the bottom kinetic energy $\langle KE\rangle$ in the shallow section. The correlation coefficient of 0.55 with a 90% confidence interval indicates a moderate relationship between turbulent dissipation rates and kinetic energy in the 'shallow' section. Only high kinetic energies ($\langle KE\rangle > 0.06\ m^2/s^2$) seem to trigger high turbulent dissipation rates; below this energy level the scatter plot suggests no evident link between $\langle KE\rangle$ and $\langle\varepsilon\rangle$. For instance, kinetic energy of $0.42 m^2/s^2$ is associated with turbulent dissipation rates at $0.5 \times 10^{-9}\ W\ kg^{-1}$ and $3.2 \times 10^{-9}\ W\ kg^{-1}$; the disparity between the two values of $\langle\varepsilon\rangle$ is roughly sixfold.

The correlation coefficient for the transition section is 0.49 with a confidence interval of 90%. In this case as well the degree of correlation indicates a moderate relationship between $\langle\varepsilon\rangle$ and $\langle KE\rangle$. However, as opposed to the shallow section, a threshold beyond which $\langle\varepsilon\rangle$ correlates wel with $\langle KE\rangle$ is absent. The highest averaged kinetic energy recorded ($\langle KE\rangle = 0.03 m^2/s^2$) generates turbulent dissipation rates of both $0.6 \times 10^{-9}\ W\ kg^{-1}$ and $1.4\times 10^{-9}\ W\ kg^{-1}$; $\langle\varepsilon\rangle$ varies by approximately twofold. Conversely no correlation holds between $\langle\varepsilon\rangle$ and $\langle KE\rangle$ in the deep section (Figure 6); as such that the highest recorded $\langle KE\rangle$ does not correspondingly produce a high $\langle\varepsilon\rangle$.

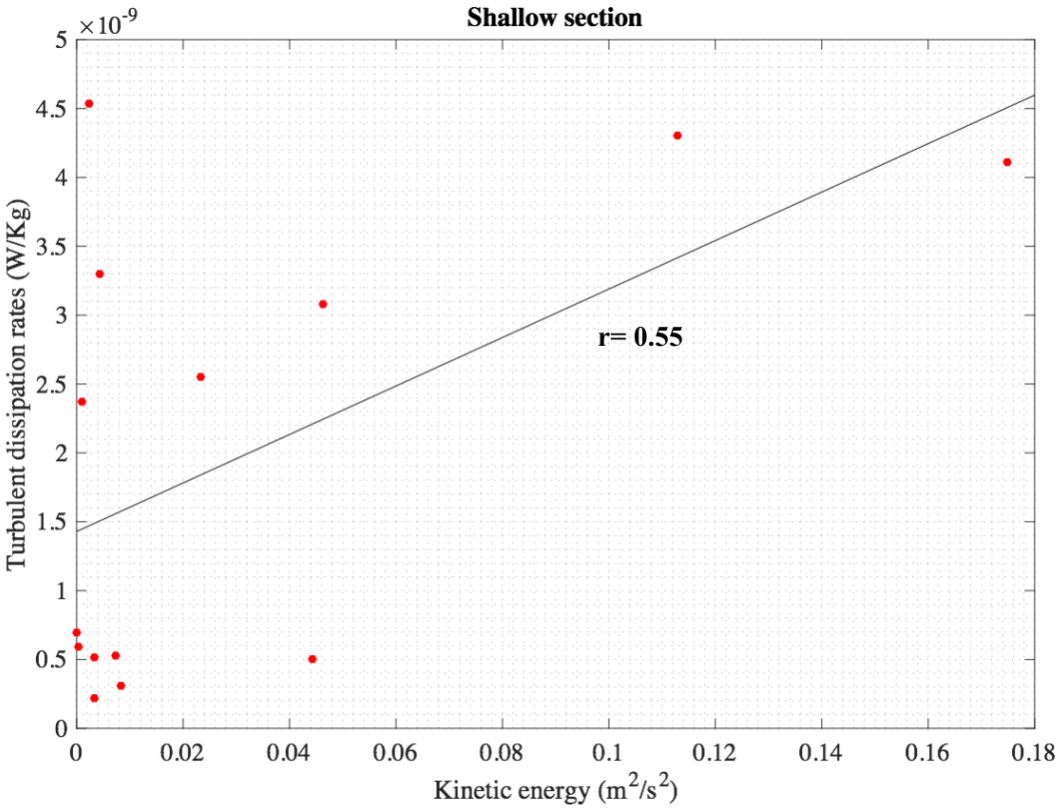

Figure 4: Turbulent dissipation rate versus kinetic energy in the deepest 100 m of the shallow section. The correlation coefficient is about 0.6

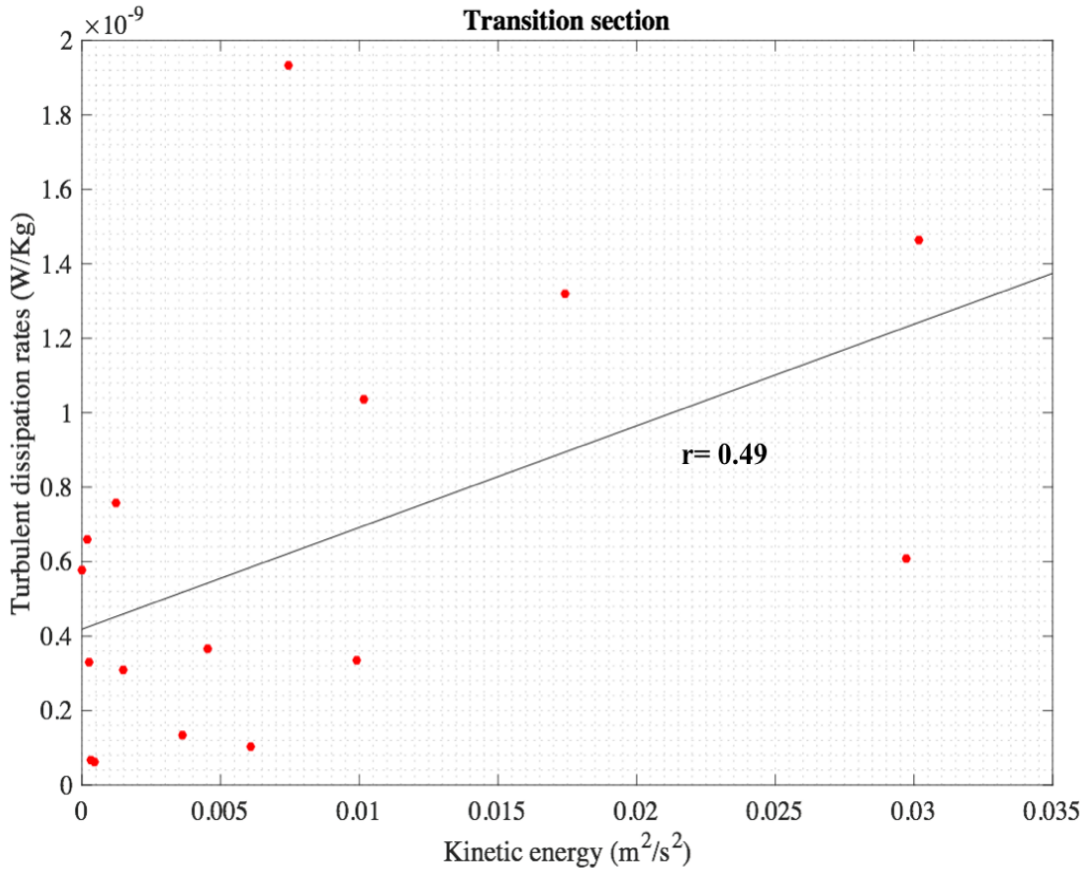

Figure 5: Turbulent dissipation rate versus kinetic energy in the deepest 100 m of the transition section. The correlation coefficient is about 0.5

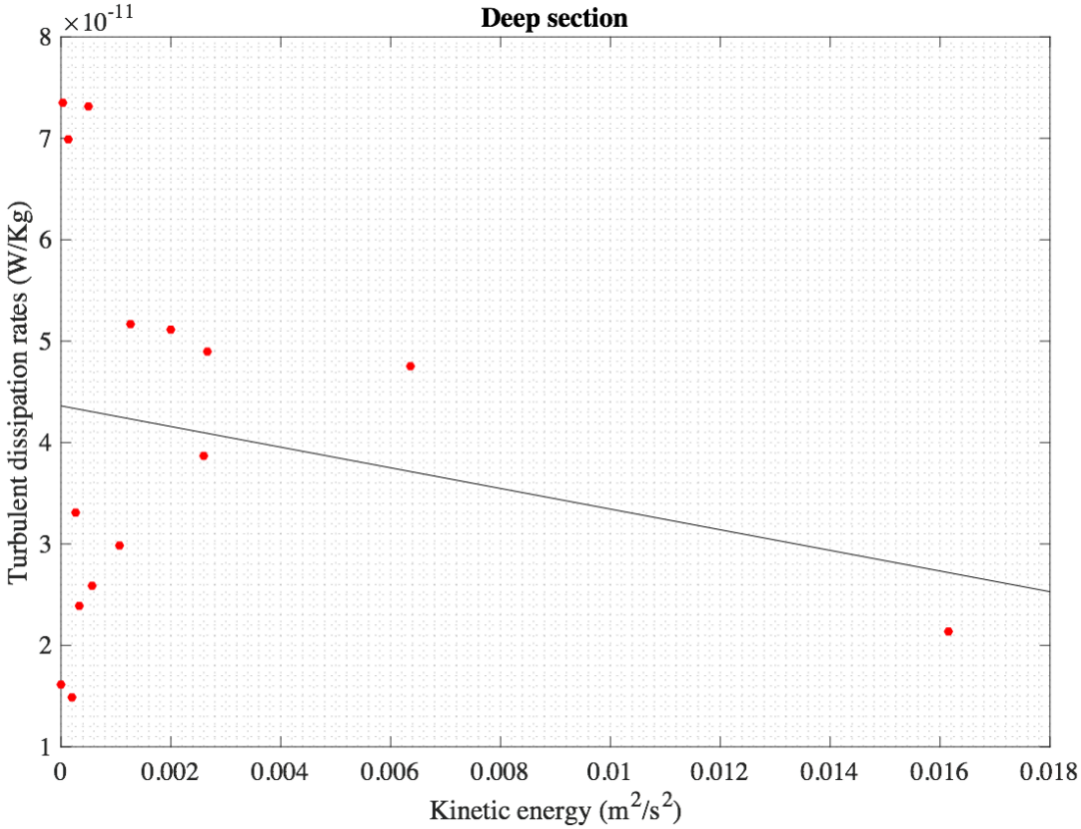

Figure 6: Turbulent dissipation rate versus kinetic energy in the deepest 100 m of the deep section. No correlation holds between the 2 datasets.

A comparison between Figures 4, 5 and 6 demonstrates that the range covered by both $\langle KE \rangle$ and $\langle \varepsilon \rangle$ shifts to smaller magnitudes when moving from the shallow to the deep section. The upper limit of the registered $\langle KE \rangle$ extends to 0.18 $W\ kg^{-1}$, 0.04 $W\ kg^{-1}$ and 0.02$W\ kg^{-1}$ for the shallow, transition and deep section respectively. The order of magnitude of $\langle \varepsilon \rangle$ is similar for both the shallow and transition section and is of $O(10^{-9})$. $\langle \varepsilon \rangle$ in the deep section is much lower and of $O(10^{-11})$.

In Figure 7, the turbulent dissipation rates from all the stations, that is across the different hydrographic sections, are binned to different depths centred at 500m, 1000m, 2000m and 3500m respectively, over a depth range of 120m. The horizontal dotted lines represent the mean ε calculated from each depth bin. The same pattern of turbulent dissipation rates is

observed along the topographic rise, consistent with the spatial distribution of ε from Figure 3 and the other hydrographic sections (appendix). The degree of turbulence is lower at depths 2000m and 3500m and of $O(10^{-11})$ while higher turbulent dissipation rates registered at 500m and 1000m are of $O(10^{-10})$. Moreover, the turbulent dissipation rates appear to be slightly elevated along the 1000m depth when compared to the 500m depth; hence hinting towards a thermocline intensified variability.

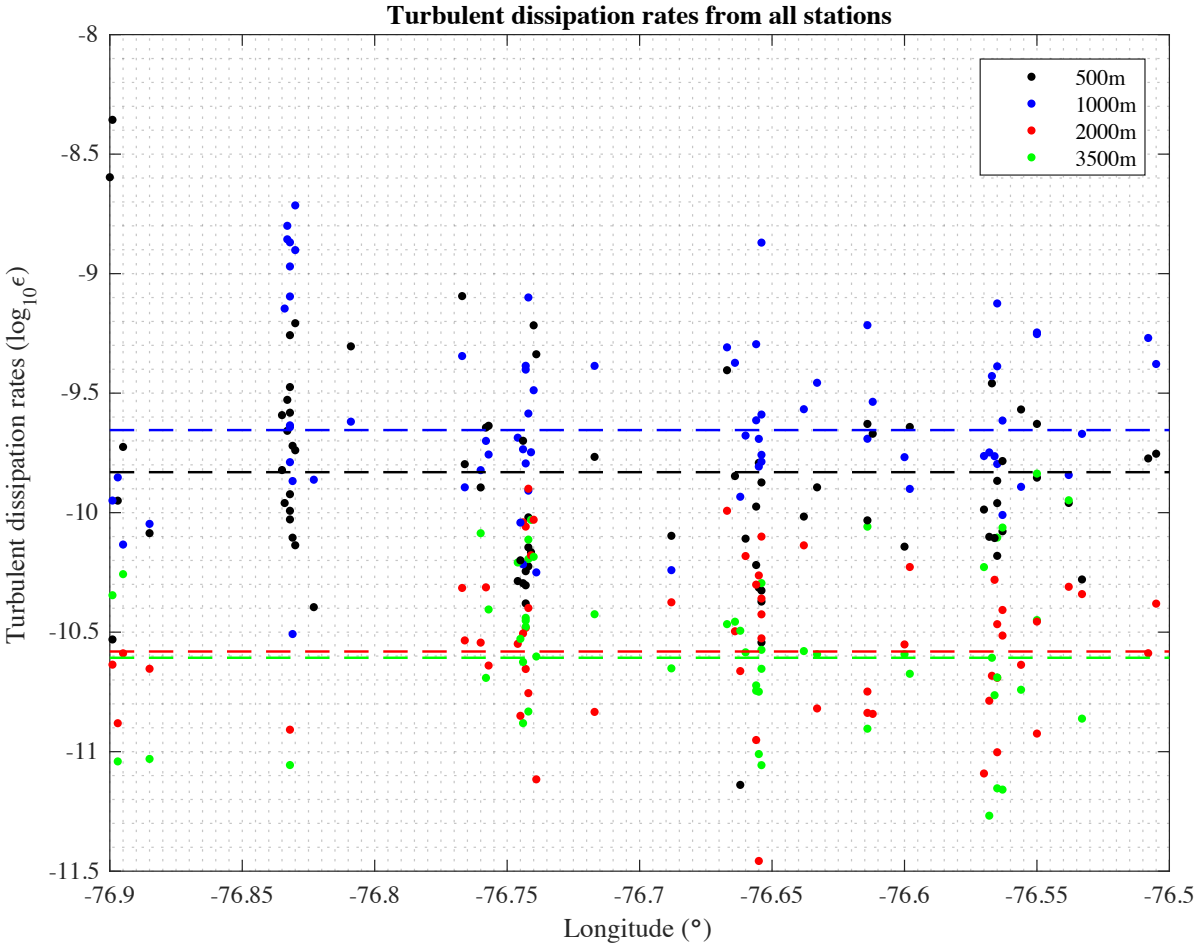

Figure 7: Turbulent dissipation rates from all stations, at different depths; 500m, 1000m, 2000m and 3500m. The horizontal lines represent the mean of the respective depth bins. Markers and line of same colour are associated with the same depth.

4. Discussion

4.1 Dependence of bottom turbulent dissipation rates on bottom kinetic energy

The restriction of high kinetic energy and high turbulent dissipation rates to the upper 1000m of the water column suggests that the eddy kinetic energy (EKE) does not penetrate through the pycnocline. Since near- bottom turbulent mixing is closely linked to the intensity of the bottom current flow (Sheen et al. 2014), the low kinetic energy registered near the seabed cannot sustain high turbulent dissipation rates. The results of this study are however still consistent with the findings of (Clément et al. 2015) who proposed a bottom generation mechanism for the dissipation of eddies off the Bahamas. The latter conducted their study in the shallow section of the topographic rise; their dataset was acquired from a mooring situated at Wba as shown in Figure 1. Considering this current study, $\langle KE \rangle$ and $\langle \varepsilon \rangle$ correlates relatively well in the shallow section of the escarpment (Figure 4) when compared to the correlation in the transition and deep region (Figures 5 and 6). (Clément et al. 2015) stated that ε is independent of KE for |v| < 8cm/s implying that a minimum value of KE= 0.064m^2s^2 would hence be required to produce a high degree of correlation between KE and ε. At this velocity threshold the bottom flow is strong enough to generate lee internal waves over the shallow section of the topographic rise (Clément et al. 2015). Only the shallow section experiences a bottom mean kinetic energy as high as $\langle KE \rangle$= 0.064m^2s^2 and indeed above this threshold the scatter plot suggests a good correlation between $\langle KE \rangle$ and $\langle \varepsilon \rangle$ (Figure 8). The next section attempts to explain why high bottom KE is registered only in the shallow section of the topographic rise.

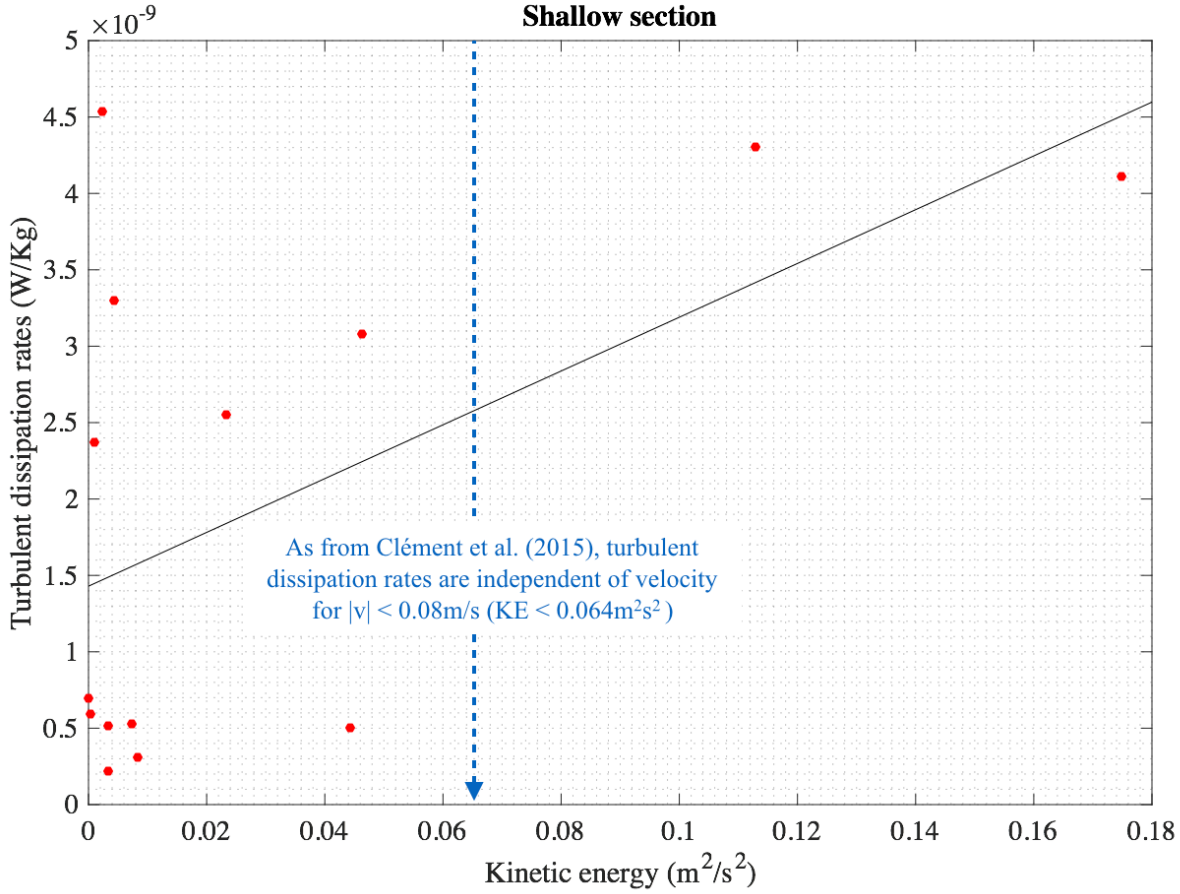

Figure 8: Same figure as Figure 4 but with the threshold specified by (Clément et al. 2015) *for good correlation between bottom turbulent dissipation rates and bottom kinetic energy*

4.2 Vertical partitioning of eddy kinetic energy

The vertical partitioning of oceanic kinetic energy is dependent on numerous physical parameters such as topographic roughness, stratification, water depth, latitude and proximity to boundaries. Following a study conducted by (Wunsch 1997) , the full depth kinetic energy is mainly divided between the barotropic and first baroclinic mode. However, the latter determined no phase coupling between the barotropic and first baroclinic mode as one approaches the western boundary in North Atlantic. In fact, the pattern of modal phase

locking changes across the Mid- Atlantic Ridge; the first two dynamical modes are coupled on the eastern side of the ridge whereas there exists a modal decoupling on the western of the ridge. The modal decoupling generates a general surface intensification of the baroclinic modes, causing the first baroclinic mode to be the most representative mode of the SSHA variability. Off the Bahamas for instance, the surface kinetic energy per unit mass is distributed as follows; 10% in the barotropic mode, 40% and 20% in the first and second baroclinic mode respectively (Wunsch 1997). A similar structure was resolved by (Richman et al. 1977) who found a strong relationship between the first baroclinic motions and altimetric SSHA.

In order to better describe the vertical structure of the westward propagating eddies impinging on the western of the Bahamas, the horizontal velocity modes of a flat- bottom linear ocean are shown in Figure 10. The presence of the permanent pycnocline at about 1000m (Figure 9) causes a surface intensification of the baroclinic modes; for example, the first baroclinic mode exhibits a much higher horizontal velocity in the upper section of the water column when compared to the deeper section (Figure 10). As stated by (Smith & Vallis 2002), a strong upper- ocean pycnocline inhibits transfer of energy to the barotropic mode; the vortices are hence trapped above this pycnocline. The surface intensified stratification seems to converge all the EKE in the upper 1000m, at the expense of EKE at depths below 1000m. This explains why high bottom KE, that is high enough to sustain the bottom generation mechanism seen in (Clément et al. 2015), is only registered in the shallow section of the topographic rise and not in the deeper section.

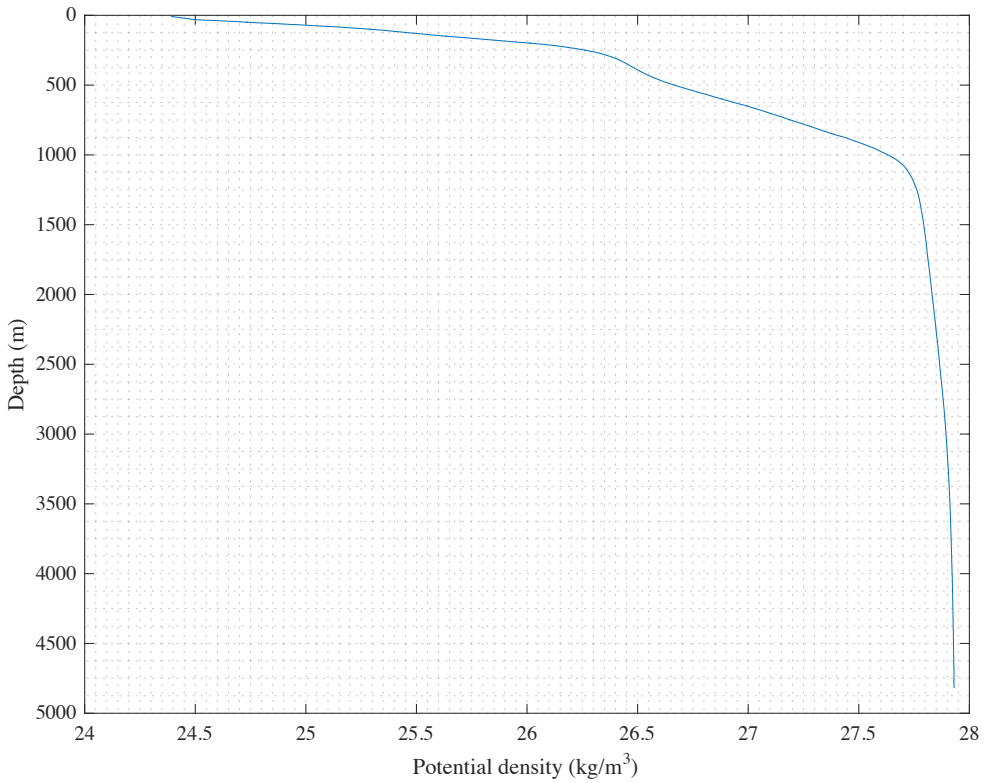

Figure 9: Potential density profile calculated and averaged from all stations. The permanent pycnocline is at around 1200m

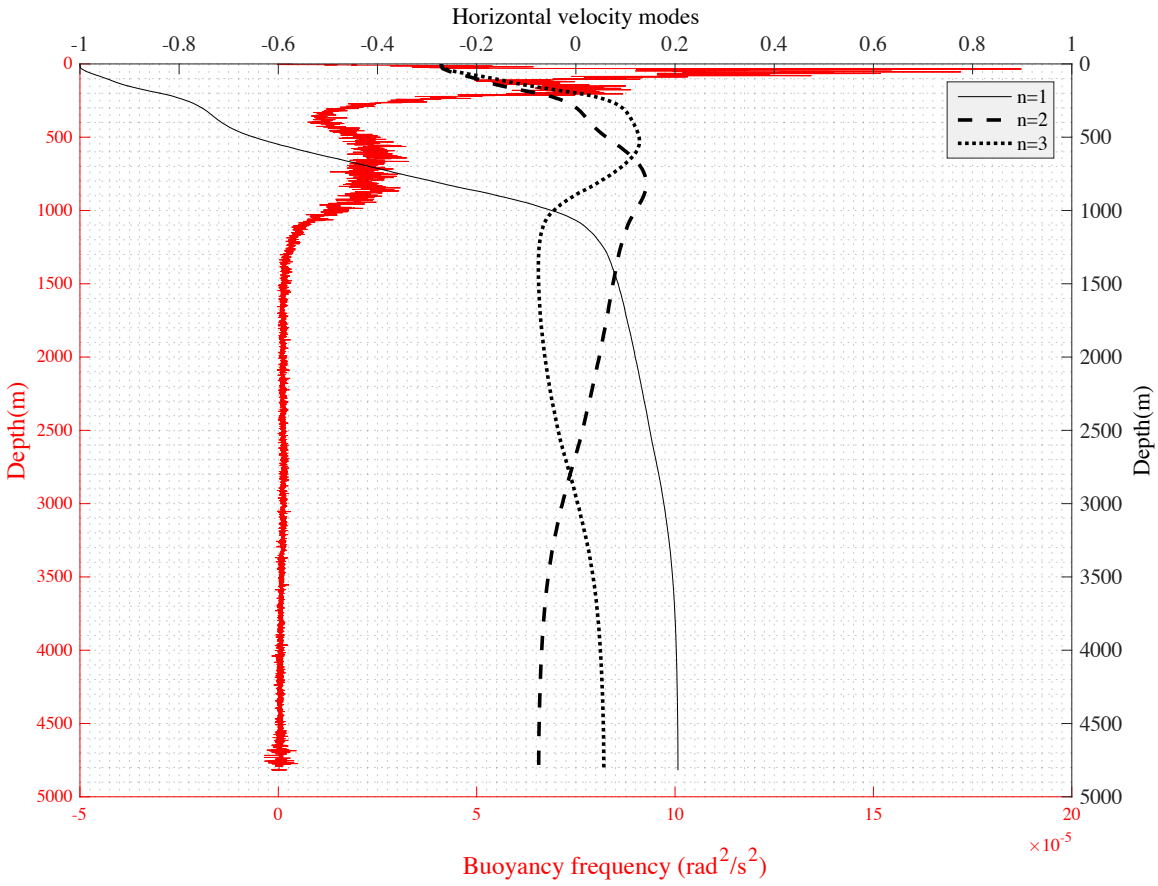

Figure 10: Averaged buoyancy frequency (red plot and red axes) from all stations and normalized horizontal velocity modes 1 to 3 (black plot and black axes).

While the relationship between SSHA and the first baroclinic mode only holds over flat topography; the correlation weakens within a Rossby radius of both the western and eastern boundaries (Szuts et al. 2012). The decline in correlation observed between the first baroclinic and SSHA as one approaches the boundaries, is also consistent with the findings of (Clément & Frajka-Williams 2014). They analysed the vertical structure of westward propagating eddies off the Bahamas and established that the dominance of the first mode diminishes significantly at 20km from the boundary whereby the variance explained by the first mode is 15%, as opposed to 52% at 500km from the boundary. Conversely the variance explained by the third mode increases when moving westward closer to the boundary. As further explained by (Clément & Frajka-Williams 2014), higher baroclinic modes are needed to resolve the complex vertical structures observed closer to the boundary at the less stratified region below 1200m. Given that the region is sheltered from the effects of the DWBC (Bryden et al. 2005), the DWBC cannot account for the deep boundary variability observed in (Clément & Frajka-Williams 2014) study. The latter hence proposed the exchange mechanism whereby energy is transferred from the first baroclinic to higher baroclinic modes. It is important to note that the deep variability (below 1200m) registered by (Clément & Frajka-Williams 2014) near the western boundary is not reflected in the deep turbulent dissipation rates of this current study. It is possible that the deep variability is so small that it does not produce intensified bottom current nor significantly change the shear at that depth. It also proves difficult to observe any type variability with this study's dataset; as opposed to data from a mooring, no timeseries analysis can be performed to study the evolution of a particular signal for instance. The aim of the next section is to propose mechanisms that allow the transfer of energy from eddies to smaller unbalanced motions at higher baroclinic modes.

4.3 Bottom generation mechanism

Firstly, the low turbulent dissipation rates registered close to the topography cannot fully support the bottom generation mechanism proposed by (Clément et al. 2015). While this hypothesis may hold for the shallow section of the topographic rise (maximum water column depth of 1000m), it does not apply to the deeper section. This might suggest a relatively small contribution from lee internal waves generation and boundary layer process towards eddy dissipation; this assumption cannot be confirmed given the relatively sparse nature of the dataset. The hydrographic sections can be analogically associated to single screenshots of the western boundary taken once a year. These sections do not necessarily capture instances when anticyclonic eddies impinge on the boundary, that is instances when the bottom kinetic energy is high. Anticyclonic eddies exhibit strong barotropic flow and relatively higher bottom mean flow as opposed to cyclonic eddies that are mainly surface intensified (Clément et al. 2015) . For example, within this dataset of 15 hydrographic sections only 2 sections recorded anticyclonic eddies over the topographic rise, while 2 other sections registered anticyclonic eddies north of 26.5°N. Besides, finescale parameterisation fails to account for dissipation related to viscous stresses at boundary layers (Waterman et al. 2014). Bottom boundary layers normally exhibit a vertical scale of O(100m) or even less (Polzin et al. 2014); a length scale which is much smaller than the vertical resolution used for finescale parameterisation in this study. Furthermore, the bottom generation mechanism as a pathway to dissipation has been largely covered by (Clément et al. 2015) and will hence not be discussed in this paper. Instead this study attempts to propose an alternative mechanism that is more likely to sustain high turbulent dissipation rates in the upper ocean, as seen in all the hydrographic sections (Figure 3 and the rest of the figures in the appendix).

4.4 Kelvin wave hydraulic control

One potential candidate responsible for high turbulence in the upper ocean is the topographic inviscid balanced dissipation mechanism proposed by (Dewar & Hogg 2010). The initial processes involved in the mechanism does not depend on viscosity but instead rely on topography. However, unlike other mechanisms supporting loss of balance through rough topography (Nikurashin & Ferrari 2009) (Clément et al. 2015), this instability catalyses small scale unbalanced flows from geostrophic flows via both smooth and rough topography. The feature only requires the presence of a no- normal flux boundary condition, as well as continuous stratification. The boundary condition constrains normal velocities at all orders, thereby triggering the formation of Kelvin waves while the continuous stratification ensures the presence of high mode and hence sufficiently slow moving Kelvin waves. The topographic high mode waves are subsequently arrested by the background balanced flow. Off western boundaries, Kelvin waves travel southward along the coast and are more likely to be arrested by the geostrophic flows of anticyclonic eddies as opposed to cyclonic ones. As stated by (Hogg et al. 2011), the near - wall disturbances and overturning identified in their simulation were only centred around a region where the northward velocities (associated with the anticyclonic eddies) exceed 0.2m/s, no such effect was registered when the cyclonic eddy interacted with the wall. The latter also specified that interior eddy velocities on the order of 0.1 m/s and thereafter amplified to 0.2 m/s, upon topographic interactions, were sufficient to induce a controlled flow.

In- situ observations, altimetry and numerical modelling centred within 500 km of the Abaco shelf have demonstrated that eddies reaching the western boundary kick off fast boundary waves that propagate equatorward (Kanzow et al. 2009). Even if low mode Kelvin waves are too fast to be arrested by the vortex flow, they still interact with the vortex field. Given the

vortex baroclinicity off the Bahamas, the interaction is modulated in the vertical and hence the resulting perturbation requires higher vertical modes (Hogg et al. 2011). These high vertical mode Kelvin waves propagate more slowly and can thus be hydraulically controlled by the vortex velocity field. As mentioned earlier, along- wall northward velocities exceeding 0.2m/s are more likely to sustain the Kelvin hydraulic control. Considering the hydrographic sections of meridional velocity off Abaco rise (appendix), most velocities approach 0.2m/s in the upper 1000m of the water column. Since the threshold for hydraulic control is reached, there is a possibility that Kelvin waves are being arrested by the northward flow. Moreover, this hypothesis is supported by the distribution of high turbulent dissipation rates within the upper 1000m of the water column.

Nevertheless, once again given the relatively sparse dataset, this theory cannot be further confirmed. For instance it cannot be determined with certainty if the disturbances are centred at the northern edge of anticyclonic eddies, as predicted by (Dewar & Hogg 2010). To validate this theory, anticyclonic eddies under investigation would have to be centred slightly south of 26.5°N while impinging the Bahamas coast. The propagation of the eddy as well as the evolution of the turbulent dissipation rate will have to be continuously analysed. At last, even in the presence of cyclonic eddies, northward meridional velocities as well as high turbulent dissipation rates are seen close to the boundary (Figure 4 in appendix). The northward velocities might be due to the shallow northward flow of the Antilles current (Bryden et al. 2005). The occurrence of high turbulence in the upper ocean, even in the presence of cyclonic eddies prevent this study from stating with certainty if the arrest of Kelvin waves is main candidate responsible for the eddy dissipation off the Bahamas.

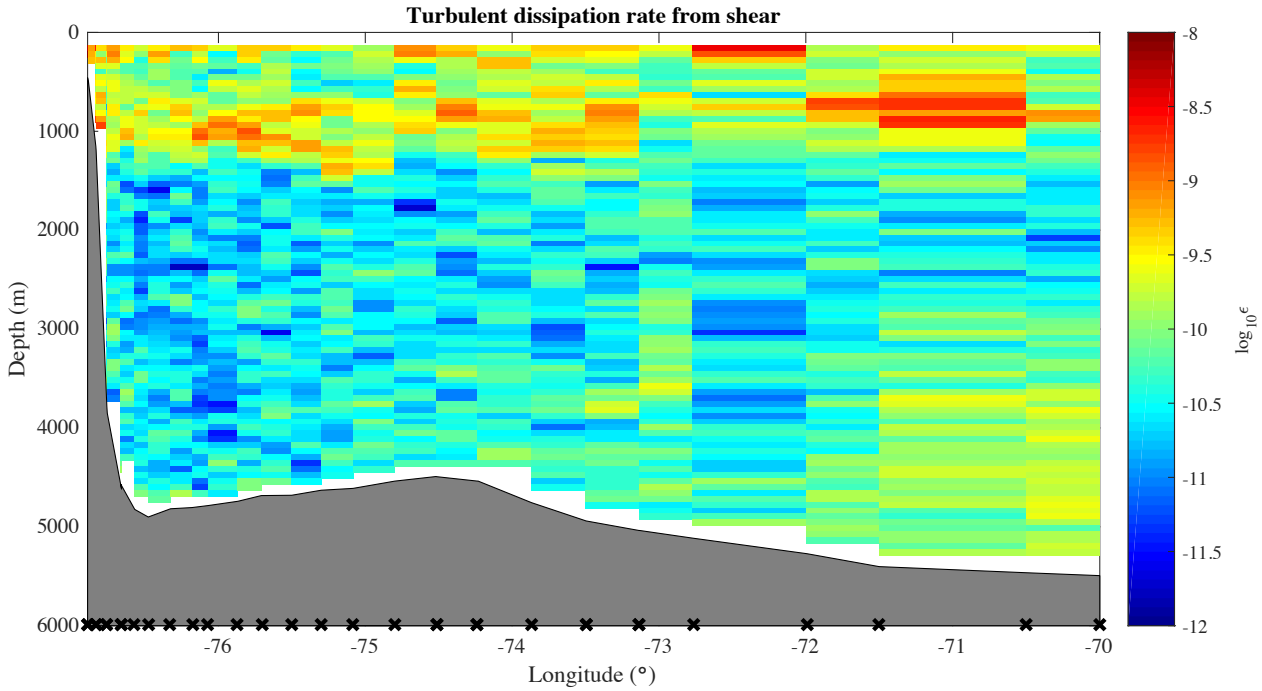

Figure 11: Similar section of turbulent dissipation rates as shown in Figure 3 but more stations further offshore are included in the section

In addition, another important feature that can hinder confirmation of the Kelvin wave hydraulic control mechanism is the distribution of high turbulent dissipation rates within the upper 1000 m further offshore. Figure 11 shows the same section as Figure 3 but with measurements extending further east. At this latitude, the Rossby radius of deformation for Kelvin waves at the surface is approximately 200 km and about 30km in the thermocline. Since higher mode Kelvin waves are more likely to be arrested by the northward flow, Kelvin hydraulic control can only occur within 30 km of the coast. The high turbulence registered east of 75°W cannot be associated with this mechanism. While the distribution of high turbulent dissipation rates within the upper 1000m of the water column can be associated with the arrest of Kelvin waves, the extension of the high turbulence further offshore does not completely agree with this dissipation mechanism. Other mechanisms not dependent on the topography, such as suppression by wind stress or frontal instabilities, could be responsible

for the eddy dissipation. None of them are discussed in this paper since the principal motivation of the study is to investigate how the western boundary may provide a sink for eddy energy.

5. Conclusion

5.1 Main findings

The spatial distribution of velocity and associated finescale derived estimates of turbulent dissipation rates off the coast of Great Abaco mainly reveals the baroclinic nature of the westward propagating eddies impinging on the boundary. A large fraction of the eddy kinetic energy is confined above the strong permanent pycnocline which is situated at about 1000m depth. This allows the eddy geostrophic flow to propagate down to the seabed only in the shallow section of the topographic rise and to produce a near bottom flow with high enough velocity to trigger near bottom turbulence and associated diapycnal mixing. Further offshore whereby the water column depth exceeds 1000m, the near bottom flow is relatively smaller and cannot sustain a similar bottom generation mechanism. On the other hand, given the restriction of higher level of dissipation to the upper 1000m of the water column and the vertical structure of velocity, Kelvin hydraulic control is suggested as a possible mechanism underpinning the dissipation of mesoscale eddies off the coast of the Bahamas. However, given the sparse nature of the dataset, this hypothesis cannot be further confirmed. This paper rather calls for a future targeted investigation of the dissipation processes that could produce high level of diapycnal mixing within the upper 1000m of the water column.

5.2 Future research

A more in- depth analysis of the dissipation pathways would involve a time series analysis of the westward propagating eddies. That is the temporal evolution of the eddy signal (both anticyclonic and cylonic for comparison) would have to be studied as it impinges on the western boundary. For instance, in the case of the Kelvin wave hydraulic control, the intensification of the northward velocities and subsequent development of hydraulic jumps would have to be observed to further confirm the dominance of the mechanism on eddy dissipation. These small scale scale structures can only be observed using a microstructure profiler. In addition, microstructure measurements would provide more accurate estimates of the turbulent dissipation rates and would thus allow the quantification of diapycnal mixing as well.

8. References:

Brearley, J. a et al., 2013. Eddy-Induced Modulation of Turbulent Dissipation over Rough Topography in the Southern Ocean. *Journal of Physical Oceanography*, 43(2009), pp.2288–2308.

Bryden, H.L., Johns, W.E. & Saunders, P.M., 2005. Deep western boundary current east of Abaco: mean structure and transport. *Journal of Marine Research*, 63, pp.35–57.

Bühler, O. & McINTYRE, M.E.M., 2005. Wave capture and wave–vortex duality. *Journal of Fluid Mechanics*, 534(2003), pp.67–95.

Clément, L. et al., 2015. Generation of internal waves by eddies impinging on the western boundary of the North Atlantic. , pp.1067–1079

Clément, L. & Frajka-Williams, E., 2014. Vertical structure of eddies and Rossby waves, and their effect on the Atlantic meridional overturning circulation at 26.5° N. *Journal of Geophysical Research*, pp.1–20.

Dewar, W.K. & Hogg, A.M., 2010. Topographic inviscid dissipation of balanced flow. *Ocean Modelling*, 32(1-2), pp.1–13.

Ferrari, R. & Wunsch, C., 2009. Ocean Circulation Kinetic Energy: Reservoirs, Sources, and Sinks. *Annual Review of Fluid Mechanics*, 41(1), pp.253–282.

Gargett, A. & Garner, T., 2008. Determining Thorpe scales from ship-lowered CTD density profiles. *Journal of Atmospheric and Oceanic Technology*, 25(9), pp.1657–1670.

Gill, A., 1982. *Adjustment under Gravity of a Density-Stratified Fluid*, London: Academic press. 177-188.

Gregg, M.C., Sanford, T.B. & Winkel, D.P., 2003. Reduced mixing from the breaking of internal waves in equatorial waters. *Nature*, 422(6931), pp.513–515.

Hibiya, T., Furuichi, N. & Robertson, R., 2012. Assessment of fine-scale parameterizations of turbulent dissipation rates near mixing hotspots in the deep ocean. *Geophysical Research Letters*, 39(24), pp.1–6.

Hogg, A.M. et al., 2011. Kelvin wave hydraulic control induced by interactions between vortices and topography. *Journal of Fluid Mechanics*, 687, pp.194–208.

Huang, R.X. & Wang, W., 2003. Gravitational Potential Energy Sinks in the Oceans. *Proceedings of the 13th'Aha Huliko'a Hawaiian Winter Workshop on Near Boundary Processes and their Parameterization*, pp.239–247.

.

Johns, W.E. et al., 2008. Variability of shallow and deep western boundary currents off the Bahamas during 2004–05: results from the 26°N RAPID–MOC Array. *Journal of Physical Oceanography*, 38(3), pp.605–623.

Kanzow, T. et al., 2009. Basinwide Integrated Volume Transports in an Eddy-Filled Ocean. *Journal of Physical Oceanography*, 39(12), pp.3091–3110.

Kunze, E. et al., 2006. Global Abyssal Mixing Inferred from Lowered ADCP Shear and CTD Strain Profiles. *Journal of Physical Oceanography*, 36(i), pp.1553–1576.

Kunze, E., Williams III, A.J. & Briscoe, M.G., 1990. Observations of shear and vertical stability from a neutrally buoyant float. *Journal of Geophysical Research*, 95(C10), pp.18127–18142.

Lee, T.N. et al., 1996. Moored Observations of Western Boundary Current Variability and Thermohaline Circulation at 26.5° in the Subtropical North Atlantic. *Journal of Physical Oceanography*, 26(6), pp.962–983.

Molemaker, M.J., Mcwilliams, J.C. & Capet, X., 2010. Balanced and unbalanced routes to dissipation in an equilibrated Eady flow. *Journal of Fluid Mechanics*, 654, pp.35–63.

Munk, W. & Wunsch, C., 1998. Abyssal recipes II: Energetics of tidal and wind mixing. *Deep-Sea Research Part I: Oceanographic Research Papers*, 45(12), pp.1977–2010.

Nikurashin, M. & Ferrari, R., 2009. Radiation and Dissipation of Internal Waves Generated by Geostrophic Motions Impinging on Small-Scale Topography: Theory. *Journal of Physical Oceanography*, 40(5), pp.1055–1074.

Park, Y.H. et al., 2014. Validation of Thorpe-scale-derived vertical diffusivities against microstructure measurements in the Kerguelen region. *Biogeosciences*, 11(23), pp.6927–6937.

Polzin, K. et al., 2002. The finescale response of lowered ADCP velocity profiles. *Journal of Atmospheric and Oceanic Technology*, 19(2), pp.205–224.

Polzin, K.L. et al., 2014. Boundary mixing in orkney passage outflow. *Journal of Geophysical Research C: Oceans*, 119(12), pp.8627–8645.

Polzin, K.L. et al., 2014. Finescale parameterizations of turbulent dissipation. *Journal of Geophysical Research: Oceans*, 119(2), pp.1383–1419.

Polzin, K.L., Toole, J.M. & Raymond, W.S., 1995. Finescale parameterizations of turbulent dissipation. *Journal of Geophysical Research: Oceans*, 25(2), pp.1383–1419.

Rhines, P.B., 1977. The dynamics of unsteady currents. In E. D. Goldberg et al., eds. *The sea*.

Richman, J.G., Wunsch, C. & Hogg, N.G., 1977. Space and time scales of mesoscale motion in the western North Atlantic. *Reviews of Geophysics*, 15(4), pp.385–420.

Saenz, J.A. et al., 2012. Mechanical power input from buoyancy and wind to the circulation in an ocean model. *Geophysical Research Letters*, 39(13), pp.1–6.

Scott, R.B. & Wang, F., 2005. Direct Evidence of an Oceanic Inverse Kinetic Energy Cascade from Satellite Altimetry. *Journal of Physical Oceanography*, 35(9), pp.1650–1666.

Sheen, K.L. et al., 2014. Eddy-induced variability in Southern Ocean abyssal mixing on climatic timescales. *Nature Geoscience*, 7(8), pp.577–582.

Smith, K.S. & Vallis, G.K., 2002. The Scales and Equilibration of Midocean Eddies: Forced–Dissipative Flow. *Journal of Physical Oceanography*, 32(6), pp.1699–1720.

Szuts, Z.B. et al., 2012. A vertical-mode decomposition to investigate low-frequency internal motion across the Atlantic at 26 N. *Ocean Science*, 8(3), pp.345–367.

Waterman, S. et al., 2014. Suppression of Internal Wave Breaking in the Antarctic Circumpolar Current near Topography. *Journal of Physical Oceanography*, 44(5), pp.1466–1492.

Wunsch, C., 1997. The Vertical Partition of Oceanic Horizontal Kinetic Energy. *Journal of Physical Oceanography*, 27(8), pp.1770–1794.

Wunsch, C. & Ferrari, R., 2004. Vertical Mixing, Energy, and the General Circulation of the Oceans. *Annual Review of Fluid Mechanics*, 36(1), pp.281–314.

Xu, Y. & Scott, R.B., 2008. Subtleties in forcing eddy resolving ocean models with satellite wind data. *Ocean Modelling*, 20(3), pp.240–251.

Zhai, X., Johnson, H.L. & Marshall, D.P., 2010. Significant sink of ocean-eddy energy near western boundaries. *Nature Geoscience*, 3(9), pp.608–612.

9. Appendix

The table below shows information about the dataset used in this study; further information of the respective dataset can be found on the NOAA website. A selection of graphs of velocity and turbulent dissipation rates from different hydrographic sections are also presented. For instance hydrographic sections that only contains one or two stations are not presented here.

Table 1: Defines the longitude covered by the hydrographic sections as the ship moved along 26.5°N. The dates when the measurements were taken is also given. Additional information on the dataset can be found on the NOAA website.

Folder name on NOAA site	Date	Longitude
GC_2001_04	28 Apr 2001	76.61°W
GC_2002_06	25- 26 Jun 2002	76.90°W- 76.61°W
GC_2003_02	11 Feb 2003	76.90°W- 76.84°W
GC_2004_09	02 Oct 2004	76.90°W- 76.67°W
GC_2005_05	08 May 2005	76.89°W- 76.66°W
GC_2006_03	18-22 Mar 2006	76.90°W- 76.61°W
GC_2006_09	28 Sept 2006	76.89°W- 76.66°W
GC_2007_09	17-18 Sept 2007	76.89°W- 76.66°W
GC_2009_04	18-19 Apr 2009	76.89°W- 76.65°W
GC_2009_11	23 Nov 2009	76.88°W- 76.83°W
GC_2011_04	15 Apr 2011	76.88°W- 76.65°W
GC_2012_02	23- 29 Feb 2012	76.83°W- 76.65°W
GC_2012_09	26 Sept 2012	76.88°W- 76.66°W
GC_2013_02	27 Feb 2013	76.89°W- 76.65°W
GC_2014_03	16-17 Mar 2014	76.88°W- 76.74°W
GC_2015_02	23 Feb 2015	76.83°W- 76.65°W

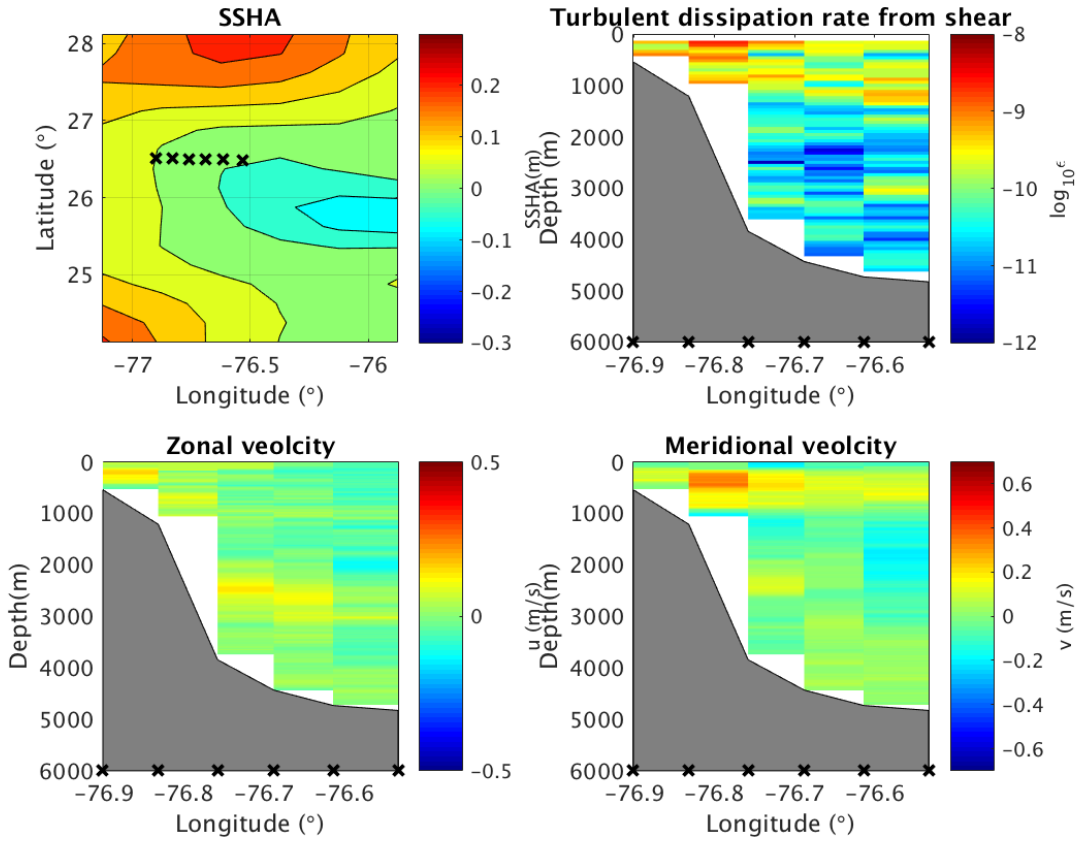

Figure 1: Hydrographic section June 2006

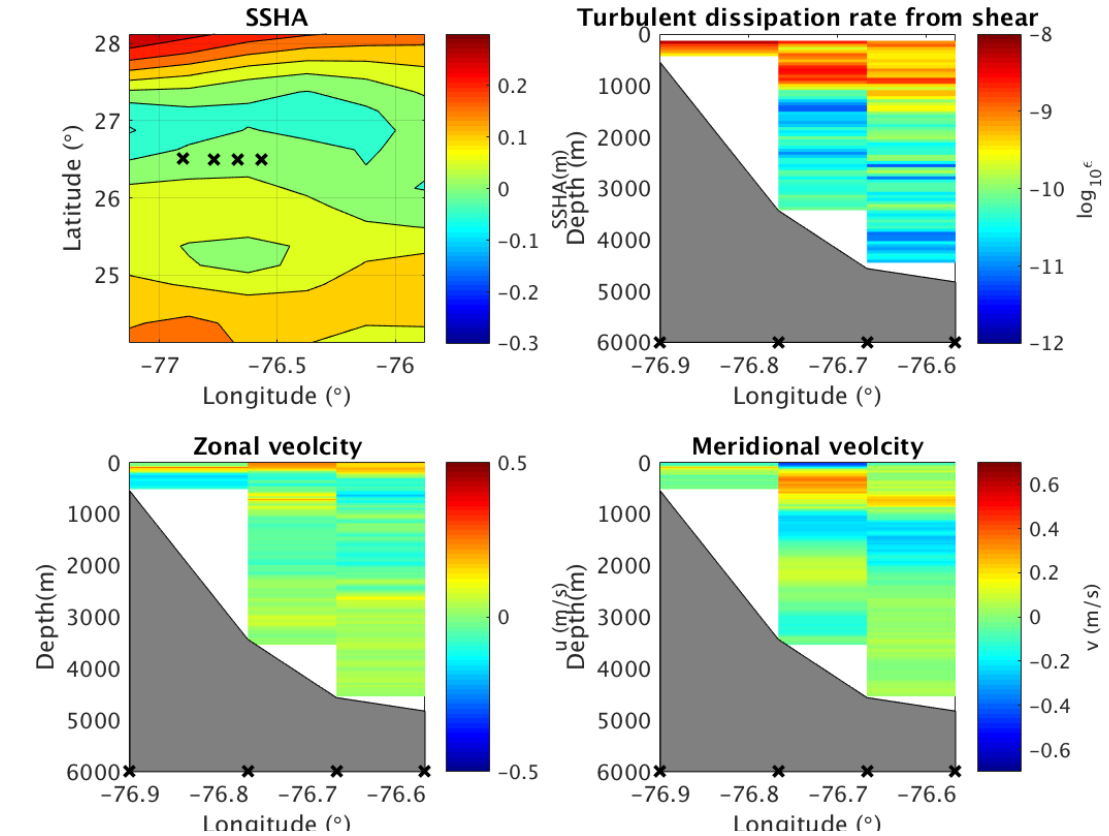

Figure 2: Hydrographic section September 2004

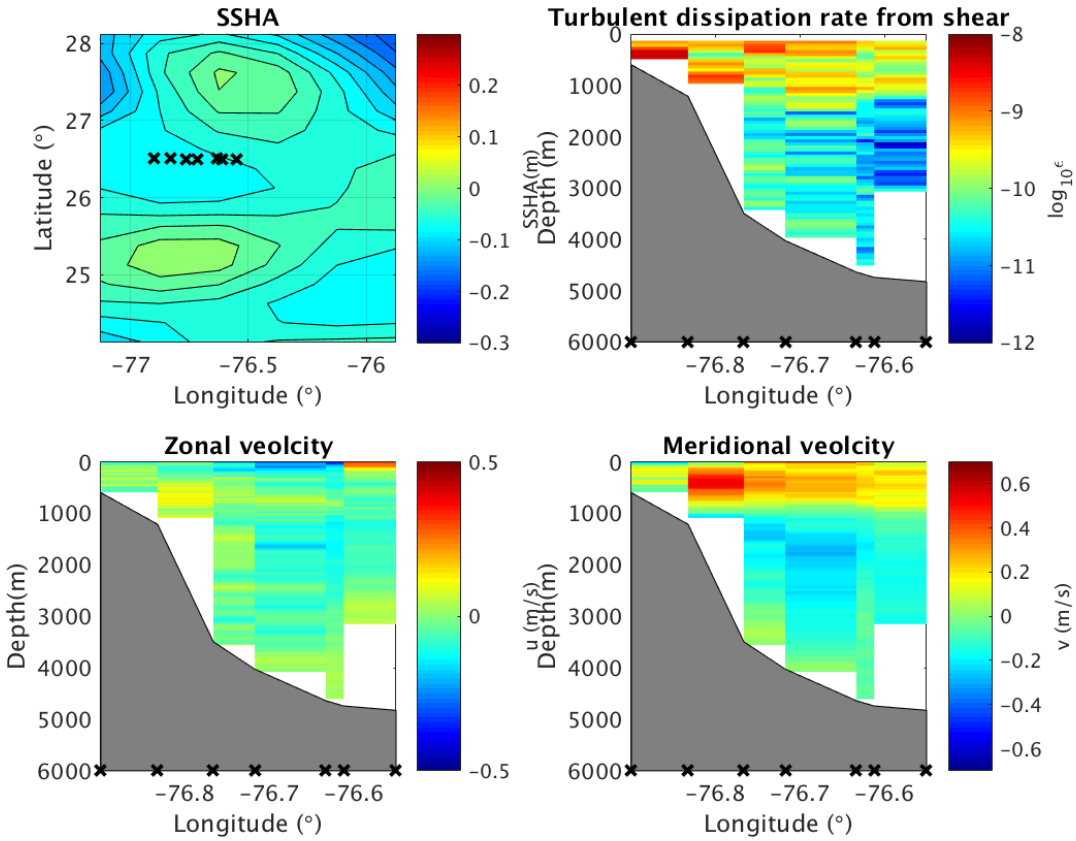

Figure 3: Hydrographic section March 2003

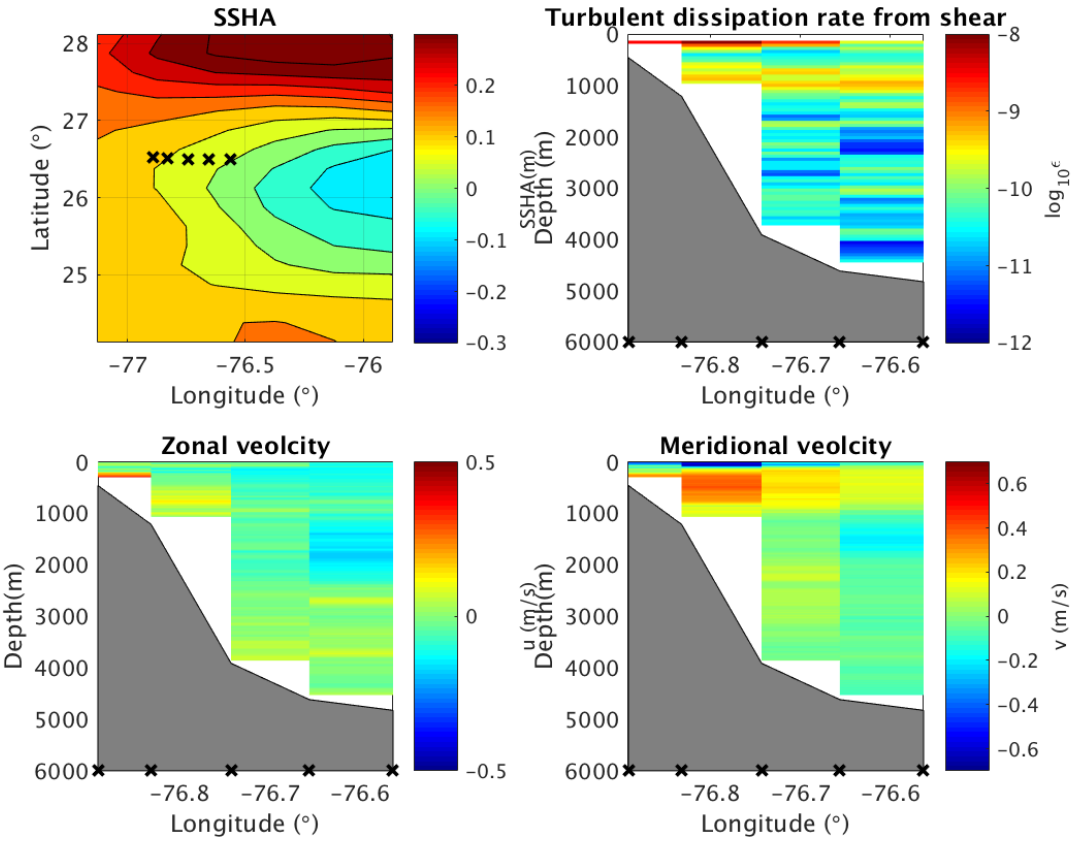

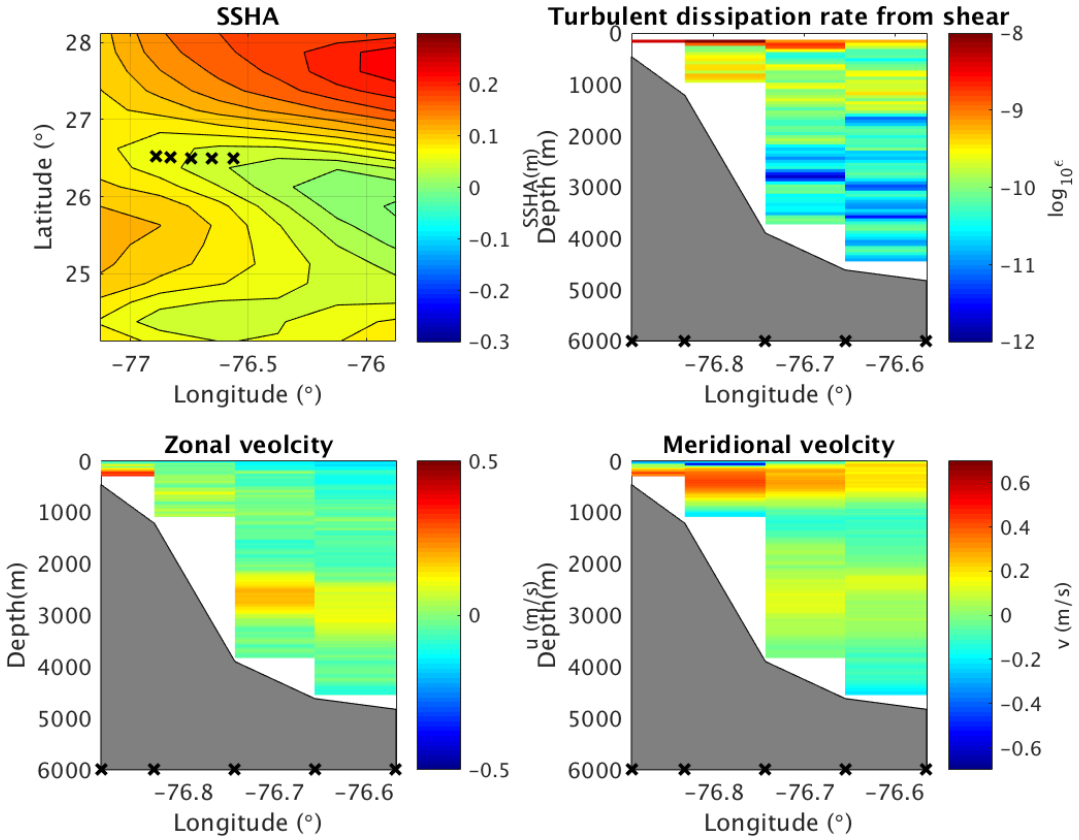

Figure 5: Hydrographic section September 2007

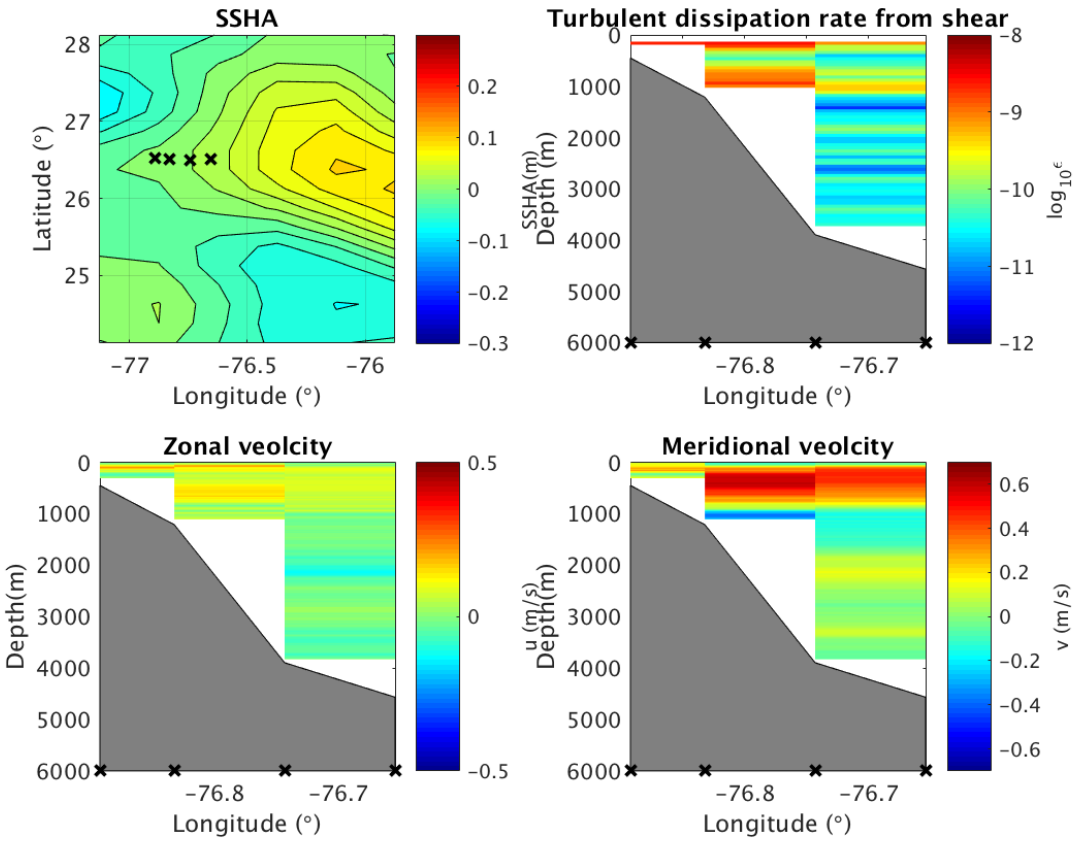

Figure 6: Hydrographic section April 2009

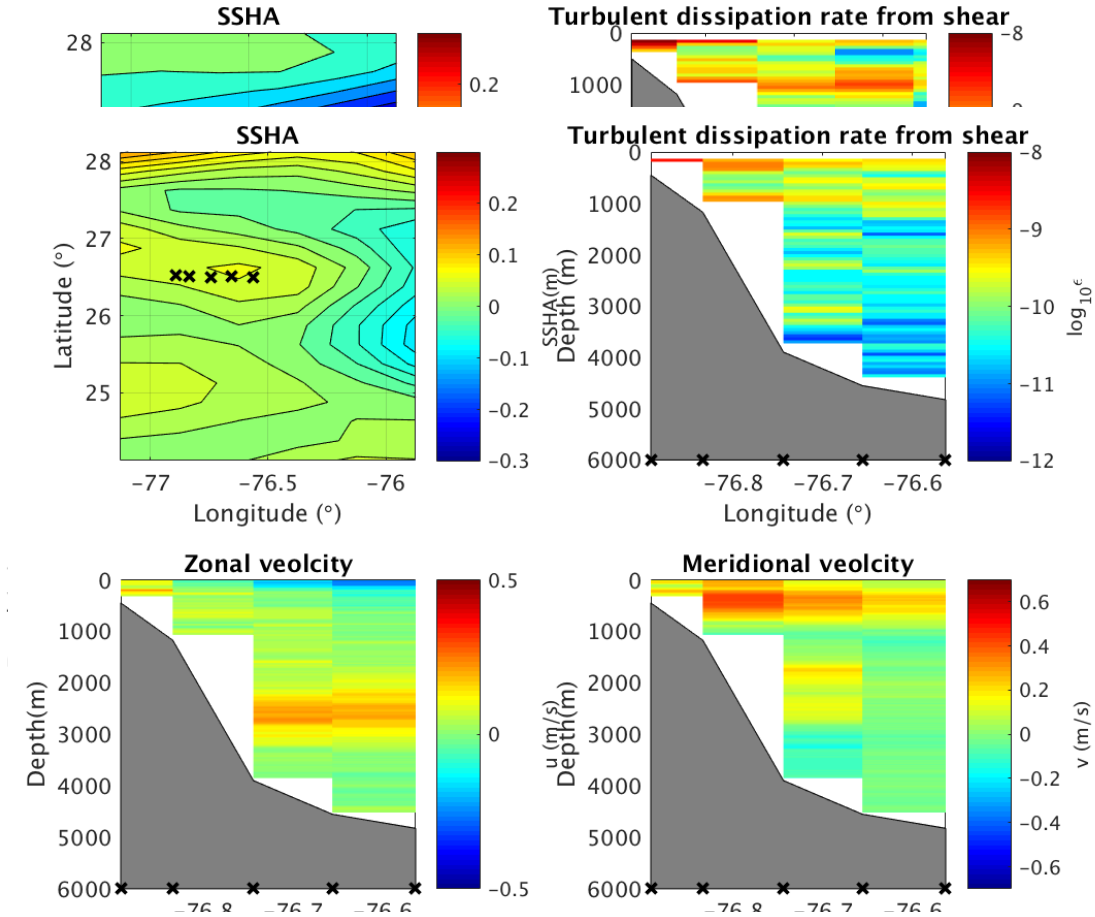

Figure 8: Hydrographic section February 2013